ELSEVIER

Journal of Nuclear Materials 266–269 (1999) 809–811

journal of nuclear materials

Pattern of ion bombardment on the poloidal divertor plates

U. Daybelge *, C. Yarim

Istanbul Technical University, Faculty of Aerospace Science, 80626 Maslak, Istanbul, Turkey

Abstract

The chaotic behaviour of particle drift orbits ending on the target plates in a poloidal divertor tokamak is studied. The source of the chaotic motion is taken to be the non-axisymmetric magnetic field perturbations. As is well known from the Chirikov–Taylor-map studies, near the separatrix, the perturbed magnetic field lines also develop a structure with various islands immersed in a chaotic sea. Following ion drift orbits across such a separatrix layer, it is shown here that particle orbits also develop both chaotic and coherent layers. Hence, the ion heat flux transported along such orbits displays a corresponding inhomogeneous distribution over the divertor plates.

Keywords: 3D edge modelling; Anomalous transport; Divertor plasma; Plasma edge physics; Scrape-off layer (SOL); Separatrix; SOL modelling; SOL thickness; SOL transport; Transport modelling; Trapped particle; Velocity distribution; Wall deposition

1. Introduction

The axisymmetric toroidal magnetic field structure of the divertor tokamak is a Hamiltonian system, which forms a sharp separatrix between closed toroidal magnetic surfaces that confine the plasma, and open field lines that divert the exhaust plasma. The occurrence of small resonant magnetic field perturbations, however, can lead to the onset of chaotic field line diffusion [1–3]. Using a *straight* three-wire model and simulating thousands of field-line trajectory circuits around the major axis, Pomphrey and Reiman [1] have shown that these deviate from flux surfaces about the divertor separatrix and wander throughout a stochastic layer [4], whose width depends on the magnitude of the perturbation. Plasma particles within the stochastic field line structure can easily escape the confinement, and be led by their open orbits to the divertor target plates, since their drift orbits may likewise become chaotic. Unlike magnetic field lines, particle orbits are also directly subject to the action of the existing electric fields. In particular, a radial electric field, which is instrumental for the L-H Mode transition [5–7], is expected to have a determining effect upon the width and the form of the chaotic drift orbit layer. Thus, in a large, long-pulse tokamak, the footprint of particle bombardment over the plates, may reflect the typical island and chaotic sea structures, a pattern indicating local excessive heat concentrations. As for the non-axisymmetric perturbation, here, we introduce a very small $n = 1$ field perturbation, whose magnitude is typical for present day tokamaks due to finite installation tolerances [1], and show its significant effect on the particle–orbit evolution. The non-axisymmetric perturbations due to magnetic field ripples [3], although typically much larger than the perturbations envisaged here, have a high toroidal mode number which reduces their effect.

2. A divertor model and the drift orbits

In cylindrical coordinates (R,z,ϕ), plasma is represented by a coil having radius R_0 and carrying a current I_p in ϕ direction. Each divertor coil located at $\pm z_d$ w.r.t. the plane of the plasma coil, and has radius $R_d = R_0 + x_d$ carries a current I_d. The magnetic field for the unperturbed configuration can be written as

* Corresponding author. Tel.:+90 212 285 3438; fax:+90 212 285 3139; e-mail:daybelge@sariyer.cc.itu.edu.tr yarim@sariyer.cc.itu.edu.tr

0022-3115/99/$ – see front matter
PII: S0022-3115(98)00605-9

$$\mathbf{B} = B_0 \frac{\hat{\phi}}{h} + (B_x^{\mathrm{p}} + B_x^{+} + B_x^{-})\hat{x} + (B_z^{\mathrm{p}} + B_z^{+} + B_z^{-})\hat{z}, \qquad (1)$$

where $x = R - R_0$, $h = R/R_0 = 1 + (x/R_0)$ and each B_x and B_z is calculated from the vector potential yielding the poloidal part of the magnetic field $\mathbf{B} = \nabla \times \mathbf{A}_\phi$

$$\mathbf{A}_\phi = I \frac{\mu_O}{\pi k} \sqrt{\frac{\rho_0}{\rho}} \left[\left(1 - \frac{k^2}{2}\right) K(k) - E(k) \right] \hat{\phi}. \qquad (2)$$

Here, K and E are complete elliptic integrals of the first and second kind, respectively. One takes $I = I_{\mathrm{p}}$, $\rho_0 = R_0$, $\rho = R_0 + x$, $\zeta = z$ for B_{p}, and $I = I_{\mathrm{d}}$, $\zeta = z - (\pm z_{\mathrm{d}})$, $\rho_0 = R_0 + x_{\mathrm{d}}$, $\rho = R_0 + x$ for $B^{\pm}$. Our calculations were carried out for $x_{\mathrm{d}} = 0$, $z_{\mathrm{d}} = 1.93$, $\gamma = I_{\mathrm{d}}/I_{\mathrm{p}} = 0.64$, $R_0 = 1/\varepsilon$, where $\varepsilon = 0.3$. We define $\lambda = \mu_0 I_{\mathrm{p}}/4\pi R_0 B_0 = 1/q$, where q is the safety factor, and take $\lambda = 0.06\varepsilon$. To this axisymmetric poloidal field we add an $n = 1$ vacuum field perturbation as $\delta B_x = \theta\lambda B_0 \exp(x/R_0)\cos\phi$, and $\delta B_\phi = -\theta\lambda B_0 \exp(x/R_0)\sin\phi$, where we choose $\theta = 0.001/\lambda$. The differential equation for guiding-center-drift-orbits for ions is given in Ref. [8] as below, where $\mathbf{b} = \mathbf{B}/B$, $\rho_{0a} = (v_{\mathrm{th}}/a)(m/eb)$ and u is normalized:

$$\frac{\mathrm{d}\mathbf{x}}{\mathrm{d}t} = u\mathbf{b} + \rho_{0a}\mathbf{b} \times \left[u^2 \mathbf{b} \cdot \nabla \mathbf{b} + \mu \nabla B + \frac{1}{2}\eta \nabla \phi + \mathbf{D} \cdot \nabla(\mathbf{b}u + \mathbf{D}) + u\mathbf{b} \cdot \nabla \mathbf{D} \right] \qquad (3)$$

parallel velocity, i.e., $u = \pm(E - 2\mu B - \eta\Phi)^{1/2}$, $\mu = V_\perp^2/(2B)$ and $\mathbf{D} = \eta(\mathbf{B} \times \nabla\Phi)/(2B^2)$ where $\eta = e\Phi_{\mathrm{ref}}/kT$. Here, E and μ are constants of motion. $B(x,z,\phi)$ and $\Phi(x,z,\phi)$ are normalized by B_0 and Φ_{ref}, respectively. In Eq. (3), we omit products involving $\boldsymbol{D}$. For computations we take $\rho_{0\mathrm{a}} = 0.01$. Using the identity $\mathbf{b}\times\mathbf{b}\bullet\nabla\mathbf{b} = -(\mathbf{bb} - \mathbf{I})\bullet\nabla\times\mathbf{b}$ one can rewrite Eq. (3) for its components along x, z, and ϕ. Substituting magnetic field from Eq. (1), drift orbits can be calculated numerically. The transversal electric field, $-\nabla\Phi$, can be modelled by using the constancy of $\xi = RA_\phi$ over the undisturbed magnetic flux surfaces, namely, one can choose

$$\phi(\xi) = 0.5\{\mathrm{Tanh}[(\xi - \xi^*)/\Delta] - 1\}, \qquad (4)$$

where (*) denotes the value at the separatrix, and vector potential $\mathbf{A}_\phi$ is due to three coils. In Eq. (4), the steepness of the potential is modeled by the parameter Δ.

3. Chaotic drift orbits

The autonomous (3) can be rewritten as

$$\frac{\mathrm{d}x}{\mathrm{d}t} = F_x(x,z,\phi;E,\mu), \quad \frac{\mathrm{d}z}{\mathrm{d}t} = F_z(x,z,\phi;E,\mu), \quad \frac{\mathrm{d}\phi}{\mathrm{d}t} = F_\phi(x,z,\phi;E,\mu), \qquad (5)$$

where E and μ are parameters. These equations correspond to a conventional 3/2 degree of freedom non-integrable Hamiltonian system [9]. For a drift orbit starting from a given point, they can be solved by numerical methods. It is interesting to determine orbits first in the absence of divertor plates and without electric field effects. For a non-integrable perturbation, the drift orbits do not cover some toroidal surfaces, but wander through a stochastic layer close to the drift surfaces of the axisymmetric problem. The width of the stochastic layer depends on the value of the perturbation parameter θ. If the width associated with the nonaxisymmetry for θ values mentioned above are small, then the introduction of plates is not as critical as in the case of a wider stochastic layer. However, the stochastic layer of particle orbits can have even a wider spread than that of the perturbed magnetic field lines, since the former do not only depend on two more parameters, such as E and μ but also are susceptible to the electric field effects. Accordingly, more complicated orbit shapes are possible, beyond the well known transiting or banana orbit forms, depending on E and μ which are fixed by initial conditions, and due to the profile of an electric potential. In Fig. 1, a Poincaré section of some particle orbits with arbitrary initial conditions, starting from the horizontal vicinity of the unperturbed separatrix at the lower-target plate is shown. The section was obtained following each orbit for 2000 toroidal circuits and by plotting a point every time it passes through $\phi = 0$ plane. The target plates are assumed to be placed at $z_{\mathrm{p}} = \pm 1.4$. Fig. 2. shows the Poincaré section of particle orbits at the lower divertor plate. The coherent part of this plot displays only part of the complicated detail. To clearly define the shape of all the structure, one needs a longer integration time than seemed appropriate.

In the presence of divertor plates, a particle would be lost upon the first intersection of its orbit with a plate. To extend the concept of the loss cones in the velocity space of a particle [10] to the stochastic case, we consider

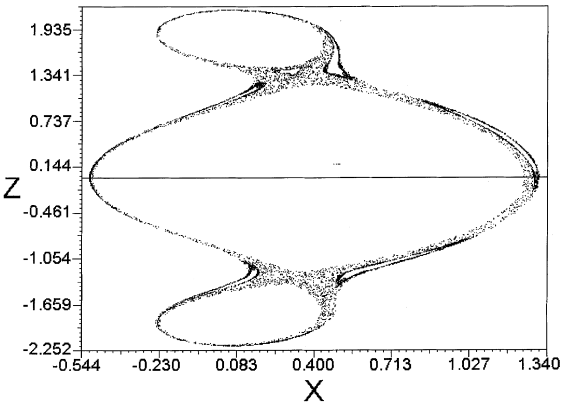

Fig. 1. Poincaré section of some randomized orbits starting from various points near separatrix.

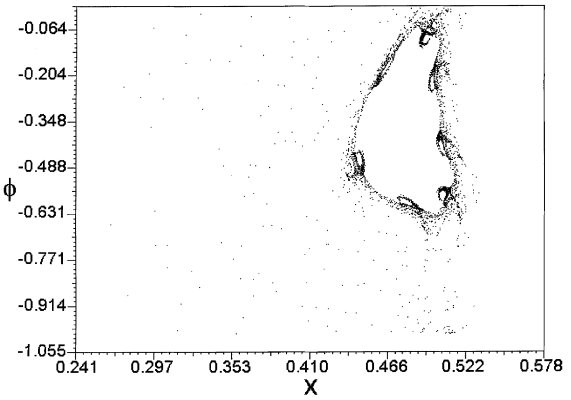

Fig. 2. Poincaré section of particle orbits at the lower divertor plate. The vertical axis denotes the toroidal angle. The orbits were started from $\phi = 0.0$ and $z = -1.4$ with different values for x.

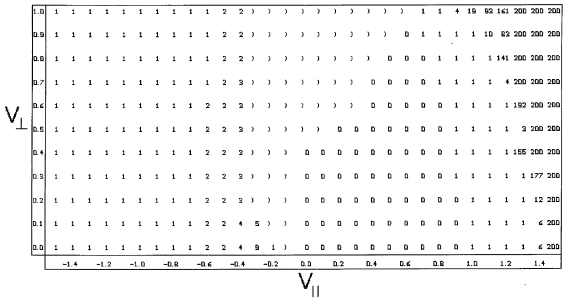

Fig. 3. Loss cone structure in the velocity space with zero electric potential. Horizontal and vertical axes denote $V_{||}$ and $V_{\perp}$, respectively. Number of toroidal transits N_{ϕ} made by each orbit starting from $x = 1.35$, $\phi = 0.0$, $z = 0.0$; with different velocities before it intersects a plate is shown. Note the gradual transition of N_{ϕ} at the borders of loss cones. Banana orbits are denoted by the symbol).

all orbits passing from a given point near separatrix at the midplane with different $V_{||}$ and $V_{\perp}$ (i.e., E and μ) values. In Figs. 3 and 4, we indicate the number of toroidal transits N_{ϕ} made (not exceeding 200) by each orbit before it intersects a plate. Some of the orbits reach one of the plates within the first toroidal transit, whereas some others can do so after thousands of transits. In this sense, these plots show us the stochastic widening of the boundaries of the loss regions. As the probability for particle collisions with a large N_{ϕ} is higher, the widening of the boundaries is an indication for the collisional replenishing of the loss cones. The same plot also shows the region for generalized banana orbits which cannot

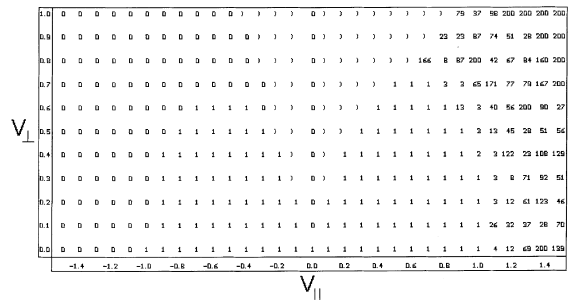

Fig. 4. Loss cone structure in the velocity space with electric potential. $\eta = 0.5$, $\Delta = 0.03$. Horizontal and vertical axes denote $V_{||}$ and $V_{\perp}$, respectively. Number of toroidal transits N_{ϕ} made by each orbit starting from $x = 1.35$, $\phi = 0.0$, $z = 0.0$; with different velocities before it intersects a plate is shown. Note the gradual transition of N_{ϕ} at the borders of loss cones. Banana orbits are denoted by the symbol).

reach any of the plates. A similar plot can be made also for a given electrical potential profile (Fig. 4.).

The BPX scrape-off width was found in Ref. [1] an order of magnitude narrower than the calculated stochastic layer width of the magnetic field lines both at the midplane and at the target plates. Our calculations indicate that the stochastic layer of particle orbits have even a wider spread than that of the field lines, if there is no electric field effect.

Our calculations indicate that for electrical field profiles with a sharper peak, particle orbits are not always squeezed together, as conventionally believed, but sometimes are also spread.

References

[1] N. Pomphrey, A. Reiman, Phys. Fluids B 4 (1992) 938.
[2] A. Punjabi, A. Verna, A. Boozer, Phys. Rev. Lett. 69 (1992) 3322.
[3] Y. Tomita, S. Seki, H. Momota, J. Phys. Soc. Jpn. 42 (1977) 687.
[4] A. Boozer, A. Rechester, Phys. Fluids 21 (1978) 682.
[5] J.W. Connor, Plasma Phys. Control. Fusion B (Suppl. (12)) 35 (1993) 293.
[6] K.C. Shaing, E.C. Crume, Phys. Rev. Lett. 63 (1989) 2369.
[7] F.L. Hinton, G.M. Staebler, Phys. Fluids B 5 (1993) 1281.
[8] R.G. Littlejohn, Phys. Fluids 24 (1981) 1730.
[9] R.Z. Sagdeev, D.A. Usikov, G.M. Zaslavsky, Nonlinear Physics, From the Pendulum to Turbulence and Chaos, Harwood Academic, Chur, 1988.
[10] M. Tendler, U. Daybelge, V. Rozhansky, Proc. 14. Int. Conf. Plasma Phys. and Contr. Nucl. Fus. Res., Wurzburg, IAEA paper D-4-8, 1992.